RSC Advances

PAPER

View Article Online
View Journal | View Issue

Cite this: *RSC Adv.*, 2020, **10**, 23675

Nanoengineering the surface of corneal implants: towards functional anti-microbial and biofilm materials†

Zohra Khatoon,[a] Irene Guzmán-Soto,[a] Christopher D. McTiernan,[a] Caitlin Lazurko,[a] Fiona Simpson,[b] Li Zhang,[c] David Cortes,[a] Thien-Fah Mah,[c] May Griffith *[bd] and Emilio I. Alarcon *[ac]

Received 23rd April 2020
Accepted 5th June 2020

DOI: 10.1039/d0ra03659e

rsc.li/rsc-advances

We report the development and use of a light-mediated *in situ* grafting technology for the surface modification of biosynthetic corneal implants with peptide-capped nanoparticles (15–65 nm). The resulting materials have antimicrobial properties in bacterial suspension and also reduced the extent of biofilm formation. Our *in situ* grafting technology offers a rapid route for the introduction of antimicrobial properties to premoulded corneal implants, and potentially other soft implant targets.

Introduction

Bacterial infection of the cornea is a serious problem as it is the most frequent cause of infectious keratitis, often resulting in ulceration of the corneal surface and even blindness if the resulting damage is permanent.[1–6] While the most common cause of bacterial keratitis is contact lens wear,[7] other causes include physical trauma (introduction of foreign bodies due to mechanical injury or ocular surgery), burns (chemical, thermal), changes in the corneal surface (from dry eye, eyelid misdirection, and exposure), altered ocular defense mechanisms (from topical and systemic immune suppression), loose sutures with adjacent infections (blepharitis and viral keratitis), and corneal edema.[8,9]

Although antibiotic eyedrops are the current mainstay treatment, they have intrinsic limitations which relate to the ease at which they can be washed from the surface by tears[10–12] and the emergence of antibiotic resistance. As such, there has been a push to develop new treatments and antimicrobial agents that circumvent these limitations. A well-documented, but rarely employed agent displaying antibacterial activity is silver. While ionic silver (Ag^+) in the form of silver nitrate, silver sulfadiazine, and other ionic silver compounds have been historically used as topical antibacterial agent, more recently silver nanoparticles (AgNP) have been explored as the next iteration of the active component of these formulations by various groups including our team.[13–15] Furthermore, through careful consideration of the size, shape, and capping agent of the employed AgNP it has been observed that one can also limit the cytotoxicity usually observed upon use of ionic Ag agents.[16]

Recently, the incorporation of antimicrobial structures, such as nanoparticles, in wearable devices, including contact lenses, has been explored as an option for imparting anti-infective properties.[17–19] While interesting, many of these materials and devices rely on impregnation or multistep chemical modifications of the implant to tether the antimicrobial component.[20,21] As such, potential clinical use of the devices can become limited due to modifications that change key physical properties of the implants or render the manufacturing process too difficult or costly.

Herein, we have developed a unique approach that allows for temporal and spatial control of the *in situ* incorporation of anti-infective AgNP onto corneal implants. The flexibility of our technology allows for surface grafting of premade implants in only minutes without the need for complex procedures or manufacturing protocols. Through evaluation of the safety and efficacy of our proposed surface modifications, we aim to highlight the promise our method holds over the more conventional approaches to the incorporation of anti-infective properties.

Results and discussion

A schematic depiction of the strategy employed for *in situ* grafting of peptide (CLKRS)-capped AgNP is presented in Fig. 1A. In our protocol, we have kept constant the ionic silver and precursor concentration within a range we have demonstrated high silver reduction with minimal side effects.[13,22] Our

[a]*Division of Cardiac Surgery, University of Ottawa Heart Institute, 40 Ruskin Street, Ottawa, Canada. E-mail: Ealarcon@ottawaheart.ca*

[b]*Centre de Recherche Hôpital Maisonneuve-Rosemont, Montréal, QC, Canada. E-mail: May.Griffith@umontreal.ca*

[c]*Department of Biochemistry, Microbiology, and Immunology, Faculty of Medicine, University of Ottawa, Ottawa, Canada*

[d]*Département d'ophtalmologie, Université de Montréal, Montréal, QC, Canada*

† Electronic supplementary information (ESI) available. See DOI: 10.1039/d0ra03659e

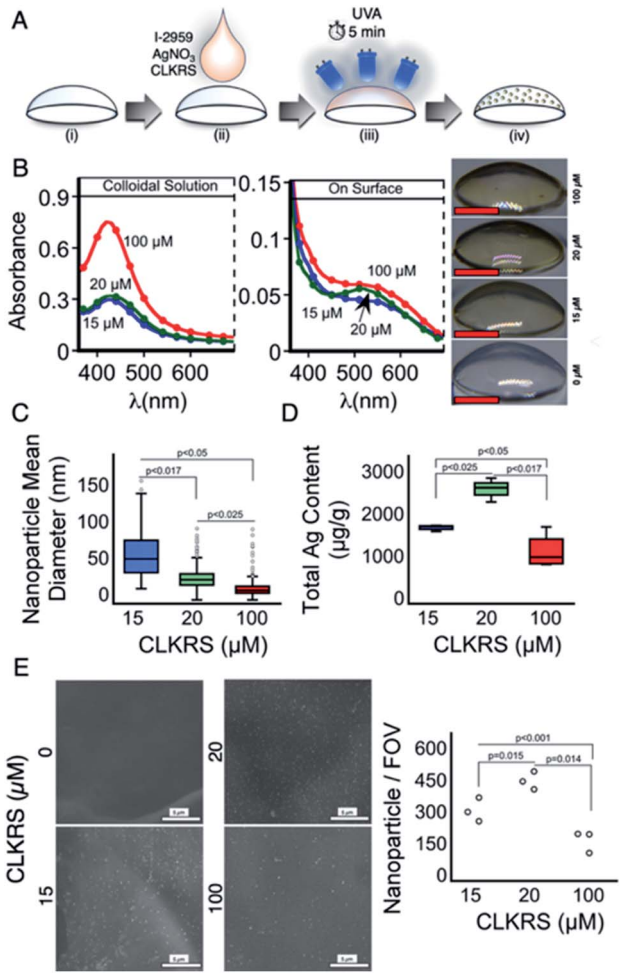

Fig. 1 Synthesis and characterization of CLKRS–AgNP grafted collagen-based corneal implants. (A) Schematic depiction for the *in situ* grafting of CLKRS–AgNP to the surface of collagen implants. The nanoparticle precursors used in the study correspond to: Irgacure-2959 (I-2959), silver nitrate ($AgNO_3$), and the CLKRS peptide. (B) Left: Surface plasmon absorption for the AgNP prepared using three different nanoparticle concentrations of the CLKRS peptide measured in colloidal solution. Middle: Surface plasmon absorption of the CLKRS capped AgNP grafted *in situ* onto the surface of the implant. Right: Representative images of the *in situ* CLKRS–AgNP grafted implants. Scale bar in all images correspond to 5 mm. (C) Average size of colloidal AgNP prepared in the presence of different concentrations of the CLKRS peptide. Diameters were calculated from measuring >100 individual particles. (D) Total silver content per g of dried implants whose surfaces were modified with nanosilver in the presence of increasing concentration of CLKRS. n = 3–4 samples per group, analysis was conducted using ICP-MS, see experimental. (E) Left: Representative CRYO-SEM images of the implant surface without and with *in situ* grafted nanosilver prepared using different CLKRS concentrations. Scale bars correspond to 5 μm in all cases. Right: Number of nanoparticles per field of view (FOV) counted on the surfaces of implants prepared using the three different CLKRS concentrations employed in this study. Counting was carried out in 3 randomly selected regions of the implants. Values in plots C and D are represented as box plots. The bars extending from the top and bottom of each box mark the minimum and maximum values with the data set that fall within an acceptable range. p values were calculated using one-way ANOVA followed by Holms post hoc analysis.

photo-grafting technique allows grafting of nanosilver onto biosynthetic premade corneal implants with only 5 min of irradiation. When comparing the plasmonic absorption for the grafted AgNP after 5 min of irradiation to that measured in colloidal solutions, see Fig. 1B left and middle; one can see a shift in the plasmonic absorption from 430 to ≈500 nm. Increasing the concentration of the peptide, however, does not change the kinetic profile for the surface plasmon band, see Fig. S1.† Further, upon *in situ* grafting the characteristic yellow colour of nanosilver is macroscopically observable in the implants as shown in Fig. 1B right. No opacity was observed in the surface modified corneal implants, which suggests that silver was fully stabilized in its nanometric form.

Preparation of the particles in the absence of the implants resulted in colloidal solutions in which increasing concentrations of CLKRS peptide resulted in AgNP with narrow size distributions and smaller diameters see Fig. 1C. This is reminiscent to recent findings reported by our group for the

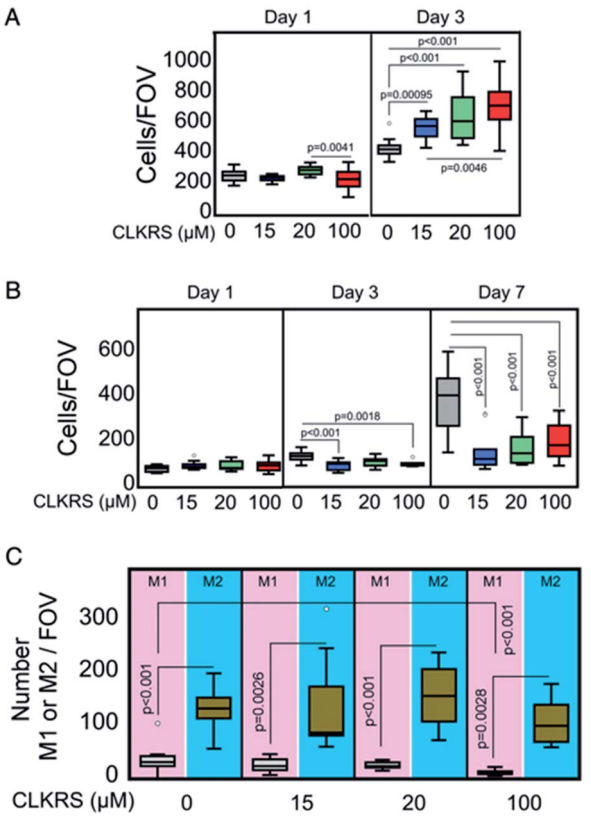

Fig. 2 *In vitro* cell compatibility assays for CLKRS–AgNP grafted corneal implants. (A) Number of human dermal epithelial cells (GFP+) per field of view (FOV) counted at 1- and 3 days post-seeding. (B) Number of macrophages per FOV counted at different time points, up to 7 days, post-seeding of bone marrow derived mouse macrophages. (C) Number of positive stained M1 or M2 macrophages per FOV counted after 7 days post-seeding on the corneal implants prepared with different concentrations of the CLKRS peptide. Values in plots are represented as box plots. The bars extending from the top and bottom of each box mark the minimum and maximum values with the data set that fall within an acceptable range. p values were calculated using one-way ANOVA followed by Holms post hoc analysis. Sample sizes were n = 4, n = 3, n = 4, and n = 4 for A, B, C and D, respectively.

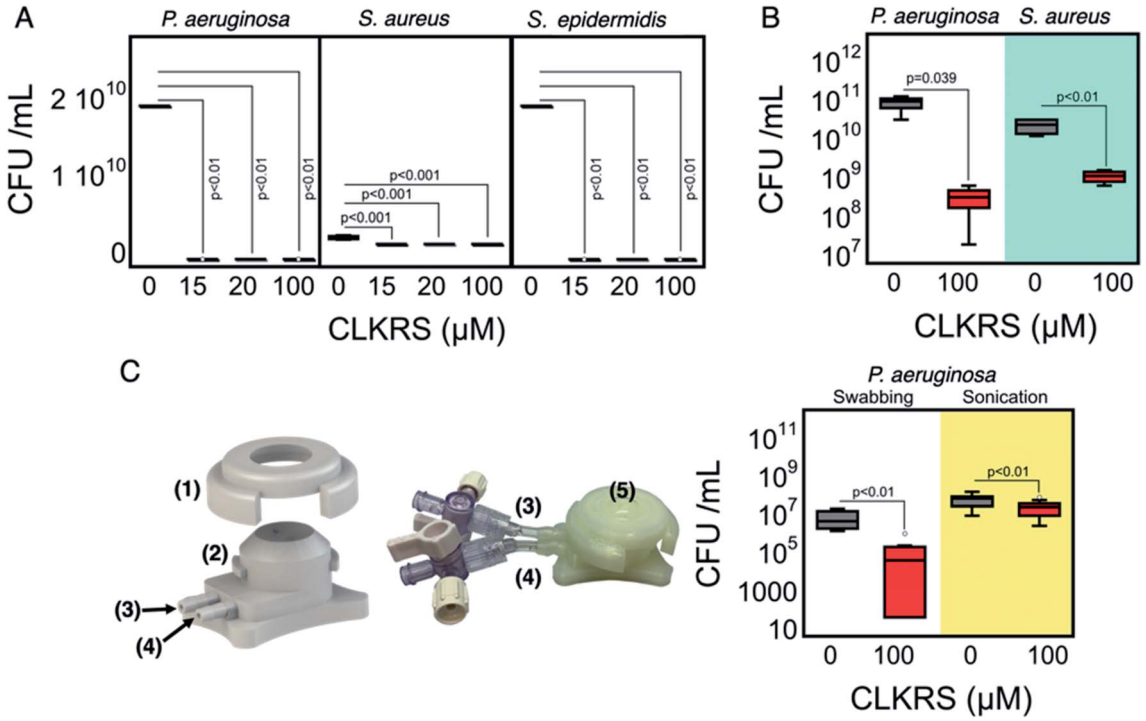

Fig. 3 Biomimetic assays for the antimicrobial properties of the CLKRS–AgNP grafted corneal implants. (A) Number of surviving colonies in solution for different bacterial strains. Colonies were counted after 16 h of incubation in LB media. Initial seeding inoculum was 1×10^5 CFU mL^{-1} from an overnight culture. (B) Number of surviving colonies. Overnight cultures of *Pseudomonas aeruginosa* were diluted with M63 medium whereas *Staphylococcus aureus* overnight cultures were diluted with TSB + 0.5% glucose. *P. aeruginosa* biofilms were grown for 6 h and staphylococci biofilms were grown for 22 h. The biofilms were cultured using an air–liquid interface at 37 °C and plated on LB agar plates. (C) Left: 3D render of the chamber used for the *ex vivo* testing of the antimicrobial corneal implants. The numbers in the figure correspond the different parts of the chamber: (1) securing cap, (2) perfusion chamber, (3) inflow channel (4) outflow channel. Middle: Photograph of an assembled chamber. The corneal implant is positioned at the centre of the chamber (5) and the fluid is pressurized to form a cornea-like curvature. Right: Number of colonies recovered from the implants (initial seeding inoculum 1×10^7 CFU mL^{-1}) after 17 h at 37 °C. Samples from the corneas were collected through swabbing or upon 15 min of sonication in sterile saline and plated on LB agar plates. In all the plots, the bars extending from the top and bottom of each box mark the minimum and maximum values with the data set that fall within an acceptable range. *p* values were calculated using one-way ANOVA followed by Holms post hoc analysis The 0 μM CLKRS groups correspond to non-grafted corneal implants. Sample sizes were $n = 4$, $n = 3$, and $n = 4$ for A, B, and C, respectively.

formation of colloidal CLKRS-capped spherical nanosilver *via* a two-step method involving capping agent exchange.[23] Measurements for the nanoparticle sizes on the biosynthetic corneal implants did not indicate significant size differences between the different experimental groups (187 ± 29 nm, 181 ± 26 nm, and 192 ± 35 nm for 15, 20, and 100 μM CLKRS, respectively). The lack of significant differences should be cautiously considered as it is limited by the CRYO-SEM imaging resolution of the system used for imaging the gels.

When measuring the loading of total silver in the implants upon photo-grafting, we also found no trend in the total silver concentration as a function of increasing peptide loading (Fig. 1D). These results are in good agreement, and almost mirror, the relative abundance of silver nanostructures which were grafted onto the surface of the various implants (Fig. 1E), as semi-quantitatively illustrated in Fig. 1E right. Furthermore, grafting of the nanoparticles onto the corneal implants does not modify the mechanical properties of the implants as depicted in Fig. S2†

Fig. 2A shows the results of a proliferation assay for human corneal epithelial cells seeded onto implants without and with a grafted layer of peptide protected nanosilver. At day 1 post-seeding, cell proliferation on nanosilver grafted surfaces prepared in the presence of 100 μM peptide was slower than that of the other tested groups. However, by day 3, cell growth on all of the nanosilver grafted groups had surpassed that of the uncoated implant. A dendritic cell assay performed ($n = 3$ mice) showed that the AgNP did not activate dendritic cells. This illustrates that the AgNP grafted onto the implants are not likely to cause inflammation, as immature dendritic cells are tolerogenic (Fig. S3†). This agrees well with the multiplex cytokine analysis carried out on the tissue surrounding the area in which the various corneas were subcutaneously implanted in a murine model, see Fig. S4.† Analysis of proliferation and polarization of mononuclear derived bone marrow macrophages, Fig. 2B, showed that in the first three days post seeding there is very little proliferation observed in either the unmodified control implant or any of the three CLKRS–AgNP modified implants. However, at 7 days post-seeding there is a marked increase in the extent of proliferation. The lag in growth may have been caused by macrophage polarization, as it has been previously documented that these cells do not proliferate well during

polarization.[24] In all cases, the tendency for monocytes to remain undifferentiated or polarized towards an anti-inflammatory or tolerogenic M2 macrophage phenotype was greater than the polarization towards pro-inflammatory M1 cells ($n = 3$) (Fig. 2C). In particular, the number of M1 macrophages was significantly reduced for the 100 μM peptide group when compared to the unmodified control. These findings are in line with the non-inflammatory activity of collagen-based biomimetic implants previously developed by our team members.[13,25]

Next, we assessed the antimicrobial potency of our *in situ* grafted implants, Fig. 3. First, we analyzed the extent to which the implants could eradicate bacteria in suspension. The data in Fig. 3A shows that upon *in situ* grafting of CLKRS–AgNP onto the implants, no surviving bacterial colonies (colony forming units per ml; CFU ml^{-1}) were detectable for any of the three bacterial strains assessed (*Pseudomonas aeruginosa* (PA), *Staphylococcus aureus* (SA), and *Staphylococcus epidermidis*). We next evaluated the ability of the surface grafted nanoparticles to delay biofilm formation, see Fig. 3B. Our results for air-liquid biofilms of PA and SA indicate that grafting of the surface with 100 μM CLKRS-capped nanosilver produced implants with reduced biofilm bacteria when compared to the unmodified control implant. Further experimentation was carried out using a human cornea-like model with a custom designed 3D printed artificial corneal chamber. The corneal implants were perfused with saline solution to form a "dome" with a geometry similar to that in the human eye, bacteria were then inoculated on the surface and then capped with a CLKRS–AgNP grafted implant. The entire system was then cultured overnight in a humidity chamber. The schematics for the 3D printed devices are shown in Fig. 3C (stl files are available from the authors upon request). Our mimetic model cornea system allows us to account for factors such as curvature and contact angle between the biofilm and the antimicrobial layer. Evaluation of the number of surviving bacterial colonies was carried out using two standard techniques namely swabbing and sonication. For both sampling techniques, quantification of the number of surviving bacterial colonies after 17 h of incubation show that the AgNP-grafted corneal implants have a significant lower number of colonies when compared to the unmodified control group (Fig. 3C right).

Conclusions

We have developed a simple and effective *in situ* method for the grafting of peptide-capped nanosilver, that within 5 minutes is capable to generating corneal implants with antimicrobial properties that were effective at eradicating *P. aeruginosa*, *S. aureus*, *and S. epidermidis*. Upon grafting with the CLKRS–AgNPs the implants were also shown to reduce the extent of biofilm formation for both *P. aeruginosa* and *S. aureus* bacteria. Future studies will look at incorporating multiarmed and multifunctional peptides for chemical tethering to other types of corneal implants; our *in situ* grafting approach presents an integrative technology that allows for excellent spatial control of nanosilver formation and could be expanded to antimicrobial grafting of other functional implants such as skin.

Experimental section

Chemicals and reagents

Silver nitrate ($AgNO_3$), 2-hydroxy-4′-(2-hydroxyethoxy)-2-methylpropiophenone (I-2959), glycine, 25% glutaraldehyde solution, sodium hydroxide (NaOH), phosphate buffered saline (PBS), sodium citrate, sodium chloride (NaCl), 4′,6-diamidino-2-phenylindole dihydrochloride (DAPI), 1,4-butanediol diglycidyl ether (BDDGE), lysogeny broth (LB) and tryptic soy broth (TSB) were purchased from Sigma-Aldrich and used without further purification. The pentapeptide CLKRS was purchased from CanPeptide. Theracol porcine type I collagen solution was purchased from Sewon Cellontech Co Ltd. Solutions were prepared with Milli-Q water, unless otherwise noted. Other cell culture media and reagents such as Dulbecco's Modified Eagle Medium (DMEM), keratinocyte media, fetal bovine serum *etc.* were purchased from Thermo Fisher Scientific unless otherwise specified.

Collagen based cornea-like hydrogel synthesis

Hydrogels of 500 μm or 200 μm thicknesses were prepared using type I medical grade porcine collagen solution. Briefly, 10% w/v collagen solutions were crosslinked using 1,4-butanediol diglycidyl ether (BDDGE) after neutralization of the collagen solution. Gels were cast into hemispherical moulds or between two glass plates and allowed to cure in a humidity chamber at 4 °C for 18–20 h. Once solidified, gels were stored in sterile PBS at 4 °C.

In situ synthesis of CLKRS capped AgNP

In situ formation of CLKRS capped AgNP was performed using 3 formulations. Briefly, collagen-based cornea like gels were washed with Milli-Q water and then dried. 2 mL of selected formulation containing 15, 20 or 100 μM of the peptide (mixture of CLKRS peptide, silver nitrate and Irgacure-2959) was then added to a weighing boat containing the gel to be modified. The solution was then irradiated in a UVA photoreactor (Luzchem) for 5 minutes. Gels were then washed with Milli-Q water and sterile PBS three times.

Surface plasmon band spectra

Surface plasmon band spectra were recorded using a SpectraMax M2 (Molecular Devices) microplate reader. Samples were prepared and kept in a 96 well plate which was then measured directly in the plate reader from 350–700 nm.

Scanning electron microscopy (SEM)

Cryo-SEM images were taken at −50 °C using a Tescan (Model: Vega II-XMU) equipped with a cold stage sample holder, a backscatter electron detector (BSE) and a secondary electron detector (SED).

Transmission electron microscopy (TEM)

TEM images of the CLKRS–AgNP solutions were prepared from 10× diluted samples. 10 μL of each of the formulations was dropped onto carbon mesh copper grids and allowed to rest for 10 min. The solution was removed, and grids were dried in a vacuum desiccator for 2–3 days. Images were obtained using a FEI Tecnai G2 F20 TEM operating at 75 kV. All samples were measured in triplicate.

Dynamic light scattering (DLS)

Hydrodynamic size and zeta potential of the CLKRS–AgNP was measured using a Malvern Zetasizer Nano ZS at room temperature in 1.0 cm path-length disposable plastic cuvettes. Samples were measured in triplicate and values correspond to the average of three measurements.

Young's modulus

Cornea-like gels with and without surface functionalization with CLKRS–AgNP were prepared as sheets and cut into strips of 3 cm length and 5 mm width. Using an Instron 3342 instrument the gels were then extended until fracture. The Young's modulus was calculated from the resulting stress–strain curve.

Microbiology assays

Bacteria cultures. Bacteria cultures were prepared using 10 μL of the bacterial suspension, initially stored in −80 °C, streaked on a LB agar plate in a 2-phase streaking pattern and incubated for 16 h at 37 °C. After single colonies had grown on the agar plate, a single colony was resuspended in 2 mL of 100% LB agar broth and incubated in an orbital shaker incubator for 16–18 h at 225 rpm and 37 °C. The treated cornea gels (500 μm thickness, 5 mm diameter) were placed in a 24-well plate and 1.5 mL of 10^5 CFU mL^{-1} of *P. aeruginosa* PA14, *S. aureus* (ATCC 25923) and *S. epidermidis* (ATCC 35984), were added in each well and incubated for 16 h. They were then plated on LB agar and quantified by CFU counting.

Biofilm assays. Biofilms of *P. aeruginosa* PA14, *S. aureus* and *S. epidermidis* were grown on the control and treated gels and quantified by counting CFU. *P. aeruginosa* cells were cultured in 5 mL LB medium whereas *S. aureus* and *S. epidermidis* were cultured in 5 mL TSB medium overnight at 37 °C. The cultures of PA14 were then diluted with M63 medium whereas *S. aureus* and *S. epidermidis* cultures were diluted with TSB + 0.5% glucose. *P. aeruginosa* biofilms were grown for 6 h and staphylococci biofilms were grown for 22 h. The biofilms were cultured in a 12-well microtiter plate using an air–liquid interface at 37 °C and then plated on LB agar plates.

Bacteria cornea like-system test. 3D printed artificial anterior chambers were used in this part of our work. Cornea-like gels (synthetic cornea) were prepared as cornea-like and flat sheets (500 μm thickness, cut into circular discs with 10 mm diameter). This biosynthetic corneas were inoculated with bacteria and then small circular disc shaped gels functionalized with CLKRS–AgNP were mounted into the cornea holders. After 17 h the upper discs were removed and abundantly washed with PBS. Using an inoculation loop the surface of the corneas was swabbed and plated on LB agar to ensure there was no prior contamination on the surface. These corneas were then inoculated with 1×10^7 CFU mL^{-1} of *P. aeruginosa* PAO1 and incubated in a humidity chamber for 17 h at 37 °C. Control and treated gels were swabbed and plated on LB agar or sonicated for 15 min in sterile saline and plated on a LB agar plate.

Cell assays

Human cornea derived epithelial cells. The *in vitro* compatibility of CLKRS-capped AgNP grafted corneas were tested using green fluorescence protein (GFP) transfected immortalized human corneal epithelial cells (HCECs).[26,27] Briefly, CLKRS-capped nanosilver corneas and unmodified control gels were fitted into a 96 well plate. The gels were washed with sterile 1× PBS for 12 h, followed by 3 h in keratinocyte serum free media (K-SFM). 2500 cells per well were then seeded into each well in K-SFM media. The cells were cultured for 3 days, with half the media being exchanged every second day. Images were captured on a NanoEntek Juli Br&Fl microscope and quantified using ImageJ.

Murine bone marrow derived macrophages and polarization assay. Macrophages were isolated as previously described[28] with ethical permission from the Animal Care and Use Committee of the Ottawa Heart Research Institute. Briefly, bone marrow-derived macrophages (BMDMs) were generated from the tibial bones of C57BL/6 female mice (8–10 weeks old). BMDMs were maintained for 1 week in DMEM with 10% FBS, 15% L929 media containing macrophage colony-stimulating factor and penicillin–streptomycin.

For the assay, BMDM precursors from female C57BL/6 mice (8–10 weeks old) were used. The wells of a 24-well culture plate were fitted with the modified and unmodified corneal implants. The hydrogel was washed 3 times with 1 mL of 1× PBS, followed by two additional 1 mL rinses with media before the seeding of cells. The BMDMs were seeded into the control wells and onto the material at a density of 20 000 cells per well in a 48-well plate. The plate was then placed in a humidified incubator at 37 °C and 5% CO_2 with the media in each well being exchanged every 48 h up to 7 days. Images were captured and quantified at day 0, 1, 3, and 7. On day 7 the wells were processed for immunofluorescence analysis to determine their polarization towards either an M1 or M2 phenotype. Briefly, media was removed, wells were washed 2× with Hank's buffer, and then cells were fixed with a solution of 4% PFA in 1× PBS at 4 °C in the dark. Fixative was removed and wells were washed 2× with NH_4Cl in PBS, waiting 7 minutes between washes. The samples were then washed 3× with 1× PBS. On the final wash 0.2% NaN_3 was added from a 2% NaN_3 stock (10 μL/1 mL). When ready for staining, samples were washed with PBS and then blocked and permeabilized using a 2% BSA in PBS solution containing 0.5% Triton X-100 for 1.5 h at RT. Primary antibodies for CD206 and CD86 were then diluted appropriately and added to the well plate to incubate overnight covered in foil at 4 °C. The next day wells were washed with 1× PBS. Secondary antibodies were diluted and added to the plate and incubated at RT covered in

foil for 1 h. After 1 h of incubation with the secondary antibodies, the wells were washed 3× with 1× PBS. The coverslips were removed from the wells and mounted onto a glass slide using Prolong™ Gold antifade reagent with DAPI (Invitrogen, P36931). Cells were imaged with a Zeiss Axiovert 200M Fluorescence microscope equipped with an AxioCam MR camera using 63× oil immersion objective. The filters employed were DAPI blue filter (Ex: 352–402 nm/Em: 417–477 nm), GFP green filter (Ex: 457–487 nm/Em: 502–538 nm), Texas Red filter (Ex: 542–582 nm/Em: 604–644 nm). For quantification, 4 random microscopic images were obtained from each well and the number of M2 and M1 macrophages was quantified using ImageJ software.

Dendritic cells. Ethical permission for this assay was obtained from the Animal Care and Use Committee of Maisonneuve-Rosemont Hospital. The tibia and femur of male, 6–12 week old, C57BL/6J mice were removed and the bone marrow was isolated.[29] Red blood cells in the marrow were lysed using ammonium chloride solution (155 mM NH_4Cl, 10 mM $KHCO_3$). Cells (1×10^6 cells per well) were seeded onto suspension culture plates in complete RPMI 1640 (RPMI-C) containing 10% containing 10% (v/v) fetal bovine serum (Wisent), 0.5 mg mL^{-1} penicillin–streptomycin–glutamine, 10 mM HEPES, 1 mM sodium pyruvate, 55 μM β-mercaptoethanol with 25 ng μL^{-1} granulocyte-macrophage colony-stimulating factor (GM-CSF) (all Gibco, ThermoFisher, Waltham, MA, USA). The cells were maintained in culture for six days and half of the media was exchanged for fresh RPMI-C containing 50 ng mL^{-1} GM-CSF on days two and three. The hydrogels (9 mm diameter, 200 μm thick) were pre-incubated overnight in 2 mL of RPMI-C before being transferred into 1 mL of fresh RPMI-C on a 24-well plate. The cells were selected using a Histodenz™ density gradient (Sigma-Aldrich, St. Louis, MO) and seeded on the hydrogels at a density of 1 × 106 cells per well in a total volume of 2 mL for materials testing. Lipopolysaccharide (1 μg mL^{-1}) was used as a positive control for BMDC activation and untreated cells were used as a negative control. The cells were labelled with direct-conjugate antibodies for CD11c, IA/IE CD40, CD80 and CD86 (Table S1†) and Zombie Aqua™ Fixable Viability Kit (BioLegend, San Diego, CA). Flow cytometry was performed with a BD LSR II and analyzed using FlowJo v10.6.1 (Becton, Dickinson & Company, Franklin Lakes, NJ, USA). The cells were gated using Zombie Aqua and CD11c as markers of a live, dendritic cell phenotype (see Fig. S5† for a gating example). A histogram of the fluorescent intensity of CD40, CD80 and CD86 was obtained and the mean fluorescent intensity was transformed into a ratio over the untreated BMDC control for analysis. The *in vitro* statistical analysis for BMDCs was performed using a one-way ANOVA with Holm–Sidak multiple comparison test (GraphPad Prism 8.4.1, GraphPad Software, LLC., San Diego, CA, USA). The unit of analysis was the mouse ($n = 3$, per group).

Animal surgery

All *in vivo* studies were conducted with ethical approval from the University of Ottawa Animal Care Committee and in compliance with the National Institutes of Health Guide for the Use of Laboratory Animals. Female C57BL/6J mice 8 weeks, each weighing 20–25 g, were chosen to assess the cytokine activation to the implanted hydrogels. The materials were prepared under sterile conditions and 6 mm circular pieces were cut. During the surgical procedure, mice were anesthetized with 3% isoflurane through a nose cone inhaler and their backs shaved and washed with betadine/70% ethanol. Paravertebral incisions were made 1.0 cm away from the vertebral column to create subcutaneous pockets by blunt dissection using hemostats. Then, the pieces of the materials were implanted ($n = 4$ per group, 4 animals for 72 h) and the incision closed with a 5.0 silk suture. Sham group underwent the surgical procedure but without the implant insertion ($n = 3$). All animals were observed for signs of inflammation and pain was managed by Buprenorphine administered post-surgery. Mice were euthanized after 72 h. Implants and skin surrounding pocket were collected to run cytokine array.

Cytokine assay

After collection at 72 h post-implantation, surrounding tissue and implant samples were homogenized and processed for protein analysis. Multiplex analysis of protein concentrations for 14 growth factors/cytokines [granulocyte-macrophage colony-stimulating factor (GM-CSF), macrophage colony-stimulating factor (M-CSF), tumor necrosis factor alpha (TNF-α), EMMPRIN, vascular endothelial growth factor (VEGF), epidermal growth factor receptor (EGF-R), interleukin 3 (IL3), interleukin 6 (IL6), interleukin 1 alpha (IL1-α), interferon gamma (IFN-γ), matrix metallopeptidase 2 (MMP2), matrix metallopeptidase 9 (MMP9), matrix metallopeptidase 12 (MMP12) and basic fibroblast growth factor (FGF-basic)] was performed with the Luminex 200 platform built on xMAP technology (Luminex Corp.) using specific magnetic beads, according to the manufacturer's instructions. All the treated samples were normalized to control which was plotted and compared amongst the treatment groups.

Silver content quantification

Silver content of treated cornea-like gels and the silver content in each of the mice organs collected were measured by inductively coupled plasma-mass spectroscopy. For the gels, samples were prepared and synthetized with CLKRS–AgNP and then freeze-dried for seven days. Similarly, the organs from mice were harvested, frozen, and freeze-dried for seven days. The samples were digested in a DigiPREP MS system (SCP Science) and silver concentration was determined by inductively coupled plasma-mass spectroscopy (ICP-MS; Agilent 7700x) by monitoring the 107 m/z signal (100 ms integration), using Argon as a carrier gas (0.85 mL min^{-1}, Ar plasma gas flow: 15 L min^{-1}). The final concentration of silver in each sample tissue were measured in μg kg^{-1} and plotted.

Statistical analysis

All tests mentioned above were repeated a minimum of 3 times in batches of 3 or 4. All data are presented as mean ± standard

deviation. The statistical analysis was performed using one-way ANOVA with Holm's post-hoc in Kaleida graph or Holm-Sidak multiple comparison GraphPad.

Conflicts of interest

The authors state there are no conflicts to declare.

Acknowledgements

This work was funded by the Canadian Institutes of Health Research (CIHR) to MG & EIA. EIA thanks the support of the Ministry of Economic Development, Job Creation and Trade for an Early Researcher Award and to the Natural Sciences and Engineering Research Council of Canada for a Discovery Grant. The authors thank Dr Francois Xavier Gueriot for providing insights on the design of the 3D holder.

References

1 L. Ung, P. J. M. Bispo, S. S. Shanbhag, M. S. Gilmore and J. Chodosh, *Surv. Ophthalmol.*, 2019, **64**, 255–271.
2 S. Watson, M. Cabrera-Aguas and P. Khoo, *Aust. Prescr.*, 2018, **41**, 67–72.
3 A. Shah, A. Sachdev, D. Coggon and P. Hossain, *Br. J. Ophthalmol.*, 2011, **95**, 762–767.
4 J. C. Hernandez-Camarena, E. O. Graue-Hernandez, M. Ortiz-Casas, A. Ramirez-Miranda, A. Navas, L. Pedro-Aguilar, N. L. Lopez-Espinosa, C. Gaona-Juarez, L. A. Bautista-Hernandez and V. M. Bautista-de Lucio, *Cornea*, 2015, **34**, 778–785.
5 G. Varaprasathan, K. Miller, T. Lietman, J. P. Whitcher, V. Cevallos, M. Okumoto, T. P. Margolis, M. Yinghui and E. T. Cunningham Jr, *Cornea*, 2004, **23**, 360–364.
6 R. Farias, L. Pinho and R. Santos, *Rev. Bras. Oftalmol.*, 2017, **76**, 116–120.
7 A. Lin, M. K. Rhee, E. K. Akpek, G. Amescua, M. Farid, F. J. Garcia-Ferrer, D. M. Varu, D. C. Musch, S. P. Dunn and F. S. Mah, *Ophthalmology*, 2019, **126**, P1–P55.
8 T. Bourcier, F. Thomas, V. Borderie, C. Chaumeil and L. Laroche, *Br. J. Ophthalmol.*, 2003, **87**, 834–838.
9 S. Egrilmez and S. Yildirim-Theveny, *Clin. Ophthalmol.*, 2020, **14**, 287–297.
10 V. Agrahari, A. Mandal, V. Agrahari, H. M. Trinh, M. Joseph, A. Ray, H. Hadji, R. Mitra, D. Pal and A. K. Mitra, *Drug Delivery Transl. Res.*, 2016, **6**, 735–754.
11 N. M. Davies, *Clin. Exp. Pharmacol. Physiol.*, 2000, **27**, 558–562.
12 S. S. Chrai, T. F. Patton, A. Mehta and J. R. Robinson, *J. Pharm. Sci.*, 1973, **62**, 1112–1121.
13 E. I. Alarcon, B. Vulesevic, A. Argawal, A. Ross, P. Bejjani, J. Podrebarac, R. Ravichandran, J. Phopase, E. J. Suuronen and M. Griffith, *Nanoscale*, 2016, **8**, 6484–6489.
14 L. J. Luo, T. Y. Lin, C. H. Yao, P. Y. Kuo, M. Matsusaki, S. G. Harroun, C. C. Huang and J. Y. Lai, *J. Colloid Interface Sci.*, 2019, **536**, 112–126.
15 T. Mokabber, H. T. Cao, N. Norouzi, P. van Rijn and Y. T. Pei, *ACS Appl. Mater. Interfaces*, 2020, **12**, 5531–5541.
16 M. Vignoni, H. de Alwis Weerasekera, M. J. Simpson, J. Phopase, T.-F. Mah, M. Griffith, E. I. Alarcon and J. C. Scaiano, *Nanoscale*, 2014, **6**, 5725–5728.
17 X. W. Tan, T. W. Goh, P. Saraswathi, C. L. Nyein, M. Setiawan, A. Riau, R. Lakshminarayanan, S. Liu, D. Tan, R. W. Beuerman and J. S. Mehta, *Antimicrob. Agents Chemother.*, 2014, **58**, 5229–5238.
18 D. Dutta, A. K. Vijay, N. Kumar and M. D. Willcox, *Invest. Ophthalmol. Visual Sci.*, 2016, **57**, 5616–5624.
19 D. Dutta, B. Kamphuis, B. Ozcelik, H. Thissen, R. Pinarbasi, N. Kumar and M. D. P. Willcox, *Optom. Vis. Sci.*, 2018, **95**, 937–946.
20 O. Gherasim, A. M. Grumezescu, V. Grumezescu, F. Iordache, B. S. Vasile and A. M. Holban, *Materials*, 2020, **13**, 768.
21 A. Besinis, S. D. Hadi, H. R. Le, C. Tredwin and R. D. Handy, *Nanotoxicology*, 2017, **11**, 327–338.
22 E. I. Alarcon, K. Udekwu, M. Skog, N. L. Pacioni, K. G. Stamplecoskie, M. González-Béjar, N. Polisetti, A. Wickham, A. Richter-Dahlfors, M. Griffith and J. C. Scaiano, *Biomaterials*, 2012, **33**, 4947–4956.
23 H. Poblete, A. Agarwal, S. S. Thomas, C. Bohne, R. Ravichandran, J. Phopase, J. Comer and E. I. Alarcon, *Langmuir*, 2016, **32**, 265–273.
24 L. Liu, Y. Lu, J. Martinez, Y. Bi, G. Lian, T. Wang, S. Milasta, J. Wang, M. Yang, G. Liu, D. R. Green and R. Wang, *Proc. Natl. Acad. Sci. U.S.A.*, 2016, **113**, 1564–1569.
25 S. McLaughlin, B. McNeill, J. Podrebarac, K. Hosoyama, V. Sedlakova, G. Cron, D. Smyth, R. Seymour, K. Goel, W. Liang, K. J. Rayner, M. Ruel, E. J. Suuronen and E. I. Alarcon, *Nat. Commun.*, 2019, **10**, 4866.
26 K. Araki-Sasaki, Y. Ohashi, T. Sasabe, K. Hayashi, H. Watanabe, Y. Tano and H. Handa, *Invest. Ophthalmol. Visual Sci.*, 1995, **36**, 614–621.
27 P. Bedford, J. Jy, L. Collins and S. Keizer, *Front. Med.*, 2018, **5**, 118.
28 J. Weischenfeldt and B. Porse, *Cold Spring Harb. Protoc.*, 2008, **2008**, pdb.prot5080.
29 A. Madaan, R. Verma, A. T. Singh, S. K. Jain and M. Jaggi, *J. Biol. Methods*, 2014, **1**, e1.